How Does a Double-Cage Single Molecule Confine an Excess Electron? Unusual Intercage Excess Electron Transfer Transition

ARTICLE *in* THE JOURNAL OF PHYSICAL CHEMISTRY A · SEPTEMBER 2010

Impact Factor: 2.69 · DOI: 10.1021/jp1056557 · Source: PubMed

6 AUTHORS, INCLUDING:

Yin-Feng Wang
Jinggangshan University
20 PUBLICATIONS **177** CITATIONS
SEE PROFILE

feng long gu
South China Normal University
104 PUBLICATIONS **1,747** CITATIONS
SEE PROFILE

How Does a Double-Cage Single Molecule Confine an Excess Electron? Unusual Intercage Excess Electron Transfer Transition

Yin-Feng Wang,[†,‡] Zhi-Ru Li,*[,†] Di Wu,[†] Ying Li,[†] Chia-Chung Sun,[†] and Feng Long Gu*[,§]

State Key Laboratory of Theoretical and Computational Chemistry, Institute of Theoretical Chemistry, Jilin University, Changchun, 130023, China, School of Chemistry and Chemical Engineering, Jinggangshan University, Ji'an, Jiangxi 343009, China, and Center for Computational Quantum Chemistry, South China Normal University, Guangzhou, 510631, Guangdong, People's Republic of China

Received: June 18, 2010; Revised Manuscript Received: August 21, 2010

To realize the chemistry of a multicage organic molecule with excess electron, as a model, by confining an excess electron inside a double-cage single molecule, the structures of $e^-@C_{24}F_{22}(NH)_2C_{20}F_{18}$ ($e^-@AB$) and $e^-@C_{20}F_{18}(NH)_2C_{20}F_{18}$ ($e^-@BB'$) are obtained at the B3LYP/6-31G(d) + 4s4p theory level. It is confirmed that the excess electron is mainly confined inside one cage with larger interior electronic attractive potential (A for $e^-@AB$ and B for $e^-@BB'$) in the ground state, while the electron is localized in the other one in the first excited state. Owing to such excess electron localizations, an interesting intercage excess electron transfer transition takes places. This intercage excess electron transfer transition exhibits five characteristics: (1) the excess electron transfer from one cage to another (A → B for $e^-@AB$ and B → B′ for $e^-@BB'$); (2) the transition is between the ground and first excited state; (3) the wavelength and strength are the largest; (4) the transition accompanies a significant charge transfer ($\Delta q > 0.8$) and molecular dipole moment change ($\Delta\mu > 20$ D); (5) the transition corresponds to SOMO → LUMO. For the transition, the oscillator strength is larger and the wavelength is shorter for the asymmetric structure ($e^-@AB$) than for the symmetric one ($e^-@BB'$), which indicates that the intercage excess electron transfer transition may be regulated by changing the size of cage. This work is useful for the designs of organic electronic sponges (porous organic electrides), organic conductor with excess electrons, and photoelectric and nanoelectronic devices.

Introduction

The charge- and electron-transfer transitions are important in the studies of the photosynthesis of plant,[1,2] molecular switches,[3,4] solar cells,[5,6] fluorescence sensors, and supramolecular assemblies.[7−9] Especially, the charge-transfer transition plays a key role in the electroluminescent[10,11] and nonlinear optics materials.[12−14]

For the excess electron systems, it should be noticed that an excess electron can be trapped in a small cavity (or a cage) formed by some surrounding polar solvent molecules in molecular cluster anions and liquids, to form solvated electrons.[15−19] The investigation of a solvated electron plays a prominent role in physics, chemistry, and biochemistry.[20,21] Stabilization and manipulation of bound electron are important in molecular clusters and nanodevices[22] and could provide new approaches to preparing conductive materials with unusual optical[23,24] or magnetic properties.[25] These excess electrons can be also trapped at anion vacancies in solid salts to form electrides.[25−27] For example, in a single-crystalline electride of $(Ca_{24}Al_{28}O_{64})^{4+}(e^-)_4$,[25−27] the high-density electrons are highly localized in the cages.

In 2005, Wu, Jiao, and their co-worker reported[28] that an electron can be trapped inside single molecular $C_{20}F_{20}$ cage forming the solvated electron $e^-@C_{20}F_{20}$. Irikura[29] designed small fluorinated cages as electron container to form cagelike single molecular solvated electron systems. More recently, we have found[30] that an electron can be trapped inside a large single molecular $C_{60}F_{60}$ cage forming the solvated electron system $e^-@C_{60}F_{60}$. All the systems reviewed above are one-cage single molecules trapping one excess electron.

As a logical consideration, can an excess electron be encapsulated inside the multicage single molecular system? How about the distribution of the excess electron in the multicage molecule? Is it localized in one particular cage or distributed among different cages? Recently, the $C_{20}F_{20}$ has been synthesized.[31] The dipole moments of the 20 exo polarized $C^{\delta+}-F^{\delta-}$ bonds are directed toward the center of the cage[19b] to form an interior electronic attractive potential (IEAP) which may be numerically illuminated by the vertical ionization potential (VDE) of 3.66 eV[28] for $e^-@C_{20}F_{20}$. Then, the structure of the symmetric double-cage single molecular solvated electron $e^-@C_{20}F_{18}(NH)_2C_{20}F_{18}$ ($e@BB'$) may be constructed, in which the two $C_{20}F_{18}$ cages are connected by two NH bridges. An asymmetric double-cage single molecular solvated electron $e^-@C_{24}F_{22}(NH)_2C_{20}F_{18}$ ($e^-@AB$) is also interesting and considered.

For the reported inorganic solid salts, the electride $(Ca_{24}Al_{28}O_{64})^{4+}(e^-)_4$ is a multielectron many-cage system,[25−27] in which the electrons confined in the inert positive frame are localized in cages and undergo hopping between neighboring cages.[27] This inspires us to consider the intramolecular excess electron localization, and excess electron localization transition as well as a possibility on the control of excess electron localization and its transition in a double-cage single organic molecule without crystal circumstance.

* To whom correspondence should be addressed. E-mail: lzr@jlu.edu.cn (Z.-R.L.); gu@scnu.edu.cn (F.L.G.).
† Jilin University.
‡ Jinggangshan University.
§ South China Normal University.

10.1021/jp1056557
Published on Web 09/30/2010

In this paper, our investigation aims at obtaining the structures of the double-cage single molecular solvated electrons e^-@AB and e^-@BB′, showing the localization of an excess electron inside one cage of the single molecule, revealing the characteristics of the excess electron transfer transitions, and exhibiting the possibility on the control of the excess electron localization transition.

Computational Details

In this work, the optimized geometric structures of the asymmetric e@AB and symmetric e^-@BB′ with all real frequencies in the ground state (X^2A) were obtained at B3LYP/6-31G(d) + 4s4p level.[30] For the purpose of comparison, the neutral $C_{24}F_{22}(NH)_2C_{20}F_{18}$ (AB) and $C_{20}F_{18}(NH)_2C_{20}F_{18}$ (BB′) were obtained at B3LYP/6-31G(d) level. The optimized geometric structures of e@AB and e^-@BB′ in the first excited state (A^2A) were obtained at CIS/6-31G(d) + 4s4p level. The calculated structures display C_2 symmetry in both the ground and excited states.

There is much literature about the controversy whether or not the density functional theory (DFT) can yield reasonably good adiabatic electron affinities (EAs)[32,33] or vertical detachment energies (VDEs). Schaefer and co-workers[33] demonstrated that DFT is indeed applicable to anions and provides EA predictions of open-shell systems. The EA and VDE of some single molecular-cage-like solvated electron systems have been obtained at the B3LYP method.[28,30] For our large double-cage solvated electron systems, the long-range corrected functionals may need to be considered. It is well-known that the VDE I and II of dianion relate to the EA and VDE of the anion, repectively. For our double-cage one-electron (special radical) systems, to find a suitable calculational method, we select the relative excess electron system $e_2@(LiF)_6$[34] and calculate its VDE I and II with different methods (see Table S1 in the Supporting Information). The Table S1 shows the VDEs at LC-BLYP level[35] are close to these at MP2 level.[34] Therefore, the VDEs, adiabatic detachment energies (ADEs), and vertical electron affinities (VEAs) of our open-shell structures were calculated at the LC-BLYP/6-311++G(d,p) + 6s6p4d level, using the following formulas:

$$\mathrm{ADE} = E[\text{opt M}] - E[\text{opt M}^-] \quad (1)$$

$$\mathrm{VDE} = E[\text{M}] - E[\text{opt M}^-] \quad (2)$$

$$\mathrm{VEA} = E[\text{opt M}^-] - E[\text{M}^{2-}] \quad (3)$$

For comparison, the results with B3LYP and HF methods are also obtained. The diffuse basis sets 4s4p and 6s6p4d are used to describe the characteristic of the excess electron.[36] The constructions and the locations of these diffuse basis sets are in the Supporting Information (see Table S2). The spin contamination is negligible. In the calculations, the expected values of spin eigenvalue $\langle S^2 \rangle$ are 0.0 for M, 0.75 for M^-, 0.0 for M^{2-} (singlet), and 2.0 for M^{2-} (triplet) species.

With regard to the calculation of the transition energies of these systems with excess electrons in the present study, choosing a proper method is important. For molecular cluster anion $(FH)_2\{e^-\}(FH)$ and neutral (HCN)···Li with excess electron,[23,24] we calculated their transition energies by CIS, TD-HF, TD-B3LYP, TD-CAM-B3LYP, and TD-LC-BLYP methods. The first transition energy results are listed in Table S3 (Supporting Information). The TD-LC-BLYP method with long-range correction is better than the conventional TD-B3LYP method. Notice that the results of CIS method are more close to the higher SAC−CI results than the TD-HF and TD-DFT results for these systems with excess electrons. The CIS/6-31G(d) calculations were performed to obtain the excess electronic absorption spectra of the e^-@AB and e^-@BB′. All the calculations were carried out with the Gaussian 03 (revision E.01) and Gaussian 09 (revision A.02) program package.[37]

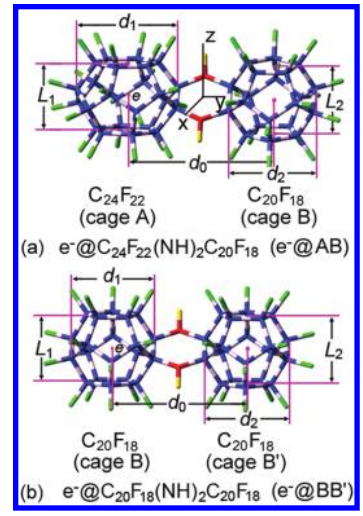

Figure 1. Optimized geometries for (a) e^-@AB and AB, and (b) e^-@BB′ complexes.

TABLE 1: Sructural Parameters (in Å), Changes in Dipole Moment ($\Delta\mu$, D) between the Ground and the First Excited State, and Intercage Charge Transfer (Δq)

	$e^-@C_{24}F_{22}(NH)_2C_{20}F_{18}$		$e^-@C_{20}F_{18}(NH)_2C_{20}F_{18}$	
	ground (X^2A)	excited (A^2A)	ground (X^2A)	excited (A^2A)
L_1	3.357 (3.371)[a]	3.328	3.447 (3.466)[a]	3.428
L_2	3.462 (3.467)	3.443	3.459 (3.466)	3.444
d_0	7.165 (7.166)	7.116	6.787 (6.797)	6.752
d_1	5.038 (5.070)	4.996	4.411 (4.432)	4.367
d_2	4.433 (4.435)	4.404	4.428 (4.432)	4.401
$\Delta\mu$	24.540		20.259	
Δq	0.843[b]		0.836[b]	

[a] The values in parentheses are for the neutral molecules. [b] For calculations, see Figure S2 in the Supporting Information.

Results and Discussion

A. Geometrical Characteristics. The optimized geometric structures of e^-@AB and e^-@BB′ shown in Figure 1 are double-cage single molecular solvated electron systems. The former is asymmetric with two different fluorinated fullerene cages of $C_{24}F_{22}$ (A) and $C_{20}F_{18}$ (B), while the latter is almost symmetric with two identical cages of $C_{20}F_{18}$ (B and B′). In each case, the two cages are connected by two NH bridges.

The sizes of the cages A and B in e^-@AB and the e^-@BB′ decrease slightly (≤0.04 Å for L and d) under the effect of the excess electron (see Table 1). For the e^-@BB′, the sizes of cage B (L_1 of 3.447 and d_1 of 4.411 Å) with the excess electron are slightly smaller than the those of cage B′ (L_2 of 3.459 and d_2 of 4.428 Å) without the excess electron. The slight decrease of the cage size slightly increases the IEAP, which is beneficial for the localization of an excess electron.

The important geometrical parameters of the e^-@AB and e^-@BB′ in the first excited state obtained at CIS/6-31G(d) + 4s4p level are also collected in Table 1. From Table 1, the sizes

TABLE 2: ADE, VDE, and VEA (eV) of the Two Structures with Different Methods with 6-311++G(d,p) + 6s6p4d Basis Set

	$e^-@C_{24}F_{22}(NH)_2C_{20}F_{18}$			$e^-@C_{20}F_{18}(NH)_2C_{20}F_{18}$		
	B3LYP	LC-BLYP	HF	B3LYP	LC-BLYP	HF
ADE	4.169			4.011		
VDE	4.343	4.032	3.355	4.157	3.660	2.816
VEA(t)[a]	1.605	1.461	0.577	1.142	1.418	0.540
VEA(s)[a]	1.329	0.099		1.127		

[a] For the dianion, t and s are triplet state and singlet state, respectively.

of the cage B′ (L_2 of 3.444 and d_2 of 4.401 Å) with the excess electron are still slightly larger than that of cage B (L_1 of 3.428 and d_1 of 4.367 Å) without the excess electron. This indicates that the excess electron prefers to be localized inside the larger $C_{20}F_{18}$ cage in the first excited state, which is different from the case in the ground state.

B. Stability in Ground State. The VDE, ADE, and VEA with B3LYP, LC-BLYP, and HF method with 6-311++G(d,p) + 6s6p4d basis set for e^-@AB and e^-@BB′ are listed in Table 2.

From Table 2, the results show that the values of VDE at B3LYP level without long-range correction are about 0.3−0.5 eV larger than those at LC-BLYP level with long-range correction and the values of VEA (triplet state for dianion) at B3LYP level are about 0.2−0.3 eV larger than these at LC-BLYP level for each of these two structures. Comparing the VDE or VEA values between HF and DFT method (B3LYP and LC-BLYP), the values at HF level are about 0.6−1.4 eV smaller than those at DFT level for these two structures. Those show that the long-range correction and the electron correlation contribution are important in the calculations.

At both LC-BLYP and B3LYP levels, the VDE is larger for asymmetric e^-@AB (4.343 or 4.032 eV) than for symmetric e^-@BB′ (4.175 or 3.660 eV), which shows that the reducibility of e^-@AB is slightly smaller than that of the e^-@BB′ and suggests that the excess electron prefers to reside in the larger cage to form the more stable cagelike single molecular solvated electron. At B3LYP level, the VDEs of e^-@AB and e^-@BB′ are lying between that of 3.66 eV[28] for $e^-@C_{20}F_{20}$ and 4.95 eV[30] of $e^-@C_{60}F_{60}$, which indicates that the reducibilities of e^-@AB and e^-@BB′ are obviously weaker than that of the $e^-@C_{20}F_{20}$ (I_h) but stronger than that of the $e^-@C_{60}F_{60}$ (I_h).

In Table 2, the ADEs of the e^-@AB and e^-@BB′ are 4.169 and 4.011 eV at B3LYP level, respectively. These show that the energy of e^-@AB or e^-@BB′ with the excess electron is lower than that of AB or BB′ without the excess electron and the AB and BB′ double-cages are favor to trap an electron.

In order to calculate the VEA values, we consider the different electronic states (singlet and triplet state) of the dianion. The EA of an anion is the binding energy of another electron to form dianion. The formed dianion may have two electronic states (singlet and triplet state). VEA(s) and VEA(t) come from singlet state and triple state of the dianion, respectively. In Table 2, the VEA(t) are larger than the corresponding VEA(s) at both B3LYP and LC-BLYP levels, which indicates that the triplet dianions are more stable than the corresponding singlet dianion. The small VEA(s) values of these structures suggest the electronic instabilities of the singlet double-cage single molecular solvated electrons. The VEA(t) is larger for asymmetric e^-@AB (1.461 eV) than for symmetric e^-@BB′ (1.418 eV) at LC-BLYP level.

The results of IPs and EAs show that the e^-@AB and e^-@BB′ have stabilities.

To assist experimentalists identify these designed double-cage-shaped single molecular solvated electron systems, the calculated infrared adsorption spectra for the two e^-@AB and e^-@BB′ and the corresponding neutral AB and BB are depicted in Figure 2. There are three prominent vibration modes: one breathing mode and two distorting modes. The breathing mode mainly presents the expanding of one cage along with the shrinking vibration of the other cage. For the distorting modes, one mainly presents expanding of one side along with the shrinking vibration of the other side for one cage in the *y*-axis direction, while the other mode presents expanding of one side along with the shrinking vibration of the other side in the *y*-axis direction for every cage and the local vibrations of the two cages are opposed-phase. These three modes are depicted in Figure S1 (Supporting Information). Under the effect of the excess electron, two significant differences for the vibrational frequency and adsorption intensity are shown. (1) The obvious red shifts of the breathing mode are observed (from 1314 (AB) to 1155 cm^{-1} (e^-@AB) and from 1317 (BB′) to 1114 cm^{-1} (e^-@BB)), which indicates that electron confinement leads to obvious softening of molecular vibrations comparing with neutral systems. (2) The IR adsorption intensities of the three vibration modes increase evidently. Especially, for the breathing mode,

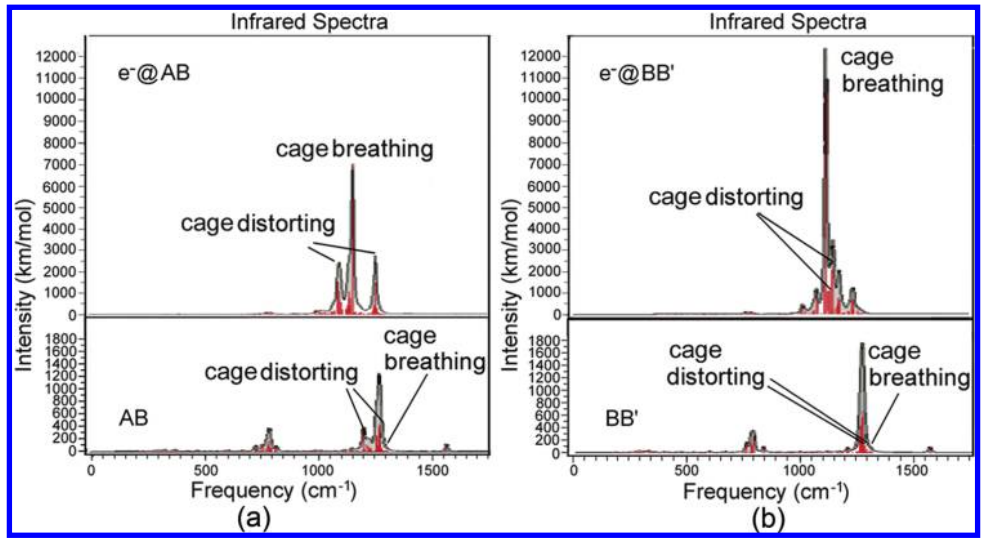

Figure 2. Calculated infrared adsorption spectra for (a) e^-@AB and AB, and (b) e^-@BB′ and BB′.

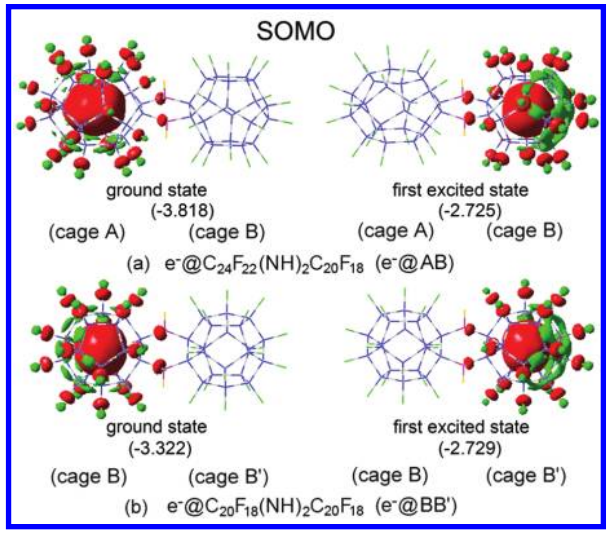

Figure 3. SOMOs (a) for e⁻@AB and (b) e⁻@BB′ in the ground state and the first excited state.

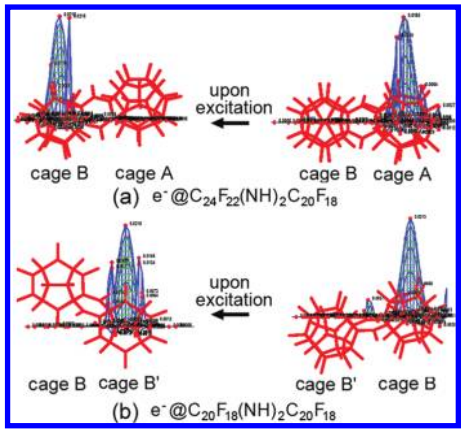

Figure 4. Spin density maps showing the excess electron transfers from one cage in the ground state to the other cage in the first excited state.

the increase is dramatic: about 4660 times from 1.5 (AB) to 6988 km/mol (e⁻@AB) and about 880 times from 14 (BB) to 12337 km/mol (e⁻@BB′).

C. Excess Electron Localization. The excess electron can be confined inside the isolated fluorinated fullerene cage.[28,30] How about the behavior of the excess electron in the double-cage molecule?

To identify the location of the excess electron for the ground states of e⁻@AB and e⁻@BB′, the SOMO of each structure is calculated and presented in Figure 3. For the asymmetric e⁻@AB, the excess electron is localized inside the larger cage (A) with larger IEAP. For the symmetric e⁻@BB′, the excess electron is localized inside one of the identical cages (B). Under the effect of the excess electron, the size of the occupied cage is slightly decreased and the perfect symmetry of the molecule (BB′) is slightly broken. The slight decrease of the cage size slightly increases the IEAP of the cage. For further confirmation of the excess electron localization inside one particular cage, the spin density was evaluated and depicted in Figure 4. The excess electron spin density distribution indicates that most of the spin density is localized in the cage A of e⁻@AB in the ground state (Figure 4a) while it is localized in the cage B (Figure 4b) for e⁻@BB′.

Also, the excess electron is localized in one of the cages in the first excited state as indicated by the SOMO (see Figure 3) and the evaluated spin density of the e⁻@AB and e⁻@BB′ in the first excited state (see Figure 4). Most of the spin density of e⁻@AB is localized inside the cage B (see Figure 4a) and most of that of e⁻@BB′ is localized within the cage B′ (see Figure 4b).

Therefore, in the ground state the excess electron is mainly confined inside one cage with larger IEAP (A for e⁻@AB and B for e⁻@BB′) while in the first excited state it is localized in the other one with smaller IEAP (B for e⁻@AB and B′ for e⁻@BB′).

D. Excess Electron Localization Transition. For practical applications, materials with large intramolecular charge transfer transition are required due to the prescribed electronic properties. To achieve this aim, electronic excitations of the investigated systems were carried out. For the e⁻@AB and e⁻@BB′, the excess electron absorption spectra at CIS/6-31G(d) level are presented in Figure 5. Comparison of these spectra reveals two obvious characteristics. (1) From e⁻@AB to e⁻@BB′, red shift from 679 to 725 nm for the first absorption peak but blue shifts (about 8−76 nm) for the second, third, and fourth ones are observed. (2) The oscillator strength of the first excited state for e@AB is about 2 times larger than that for e@BB′ (0.17 for e⁻@AB and 0.08 for e⁻@BB′). At the same time, the oscillator strength for the third absorption peak increases about 3 times from e⁻@AB (0.04) to e⁻@BB′ (0.13), and these for the second and fourth absorption peaks are in a narrow range of 0.13−0.15. Therefore, we have chosen the first four low-lying transitions for the following discussions.

The diagram of these selected electronic excitations and the contour plots for their corresponding molecular orbitals (MOs) are presented in Figure 6. These MOs come from eigenvectors of the CIS calculation. From the point of view of maximal

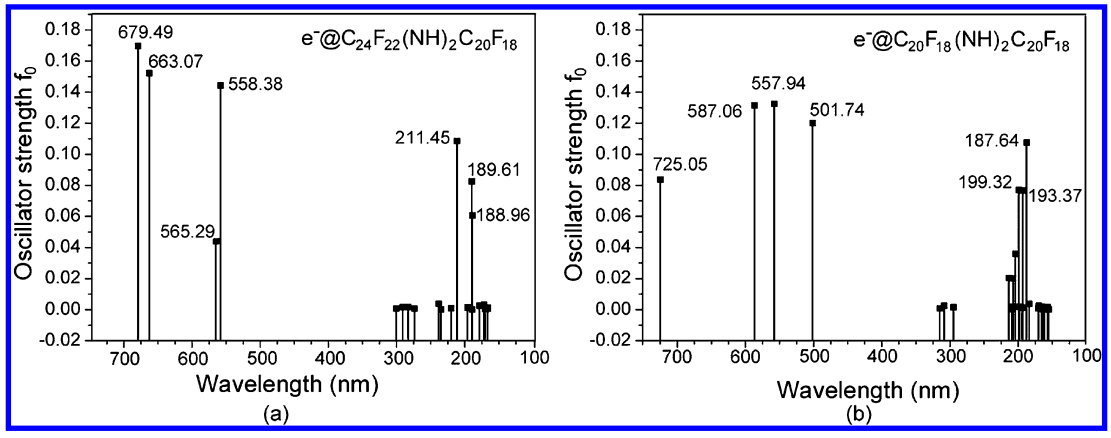

Figure 5. Electronic absorption spectra for (a) e⁻@AB and (b) e⁻@BB′ complexes.

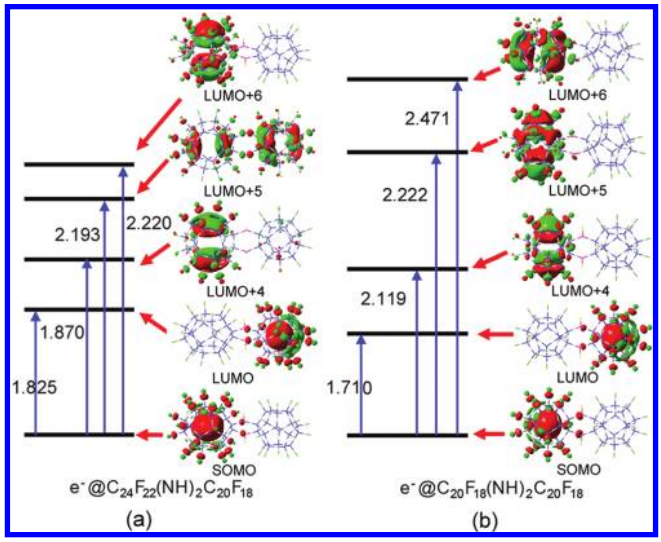

Figure 6. Energy diagram for the first four excited states (excitation energies in eV) at CIS/6-31G(d) level for (a) e^-@AB and (b) e^-@BB′. The MOs relating to the electronic transition are shown. The first electronic transition is interesting intercage electronic transfer transition.

TABLE 3: First Transition Energy (in eV) in the Electron Absorption Spectrum

	first transition energy	ref
e^-@AB	1.825	this work
e^-@BB′	1.710	this work
(HCN)···Li	1.331	24
$12CaO·7Al_2O_3$ crystal	~1.0	26
Na_nF_{n-1} ($n \leq 6$)	0.95−1.5	38
$(H_2O)_n^-$ ($n \rightarrow \infty$)	1.977; 1.947	6

intramolecular charge transfer, the electronic transitions associated with the first excited state are the most interesting for both the considered systems. This special electron transition is localized from one cage to another (A → B for e^-@AB and B → B′ for e^-@BB′) and the electronic excitation corresponds to s → s transition with the energy of 1.825 eV for the e^-@AB or 1.710 eV for the e^-@BB′. For both double-cage single molecular systems, the confined excess electron is directly encapsulated by the positively charged C cage and undergoes large attractive potential, which is different from the multielectron many-cage electride of $(Ca_{24}Al_{28}O_{64})^{4+}(e^-)_4$.[25−27] From Table 3, the intercage transition energies of the two considered systems are larger than that of $12CaO·7Al_2O_3$ crystal (about 1.0 eV).[27] For the other systems with excess electrons, for example, the first transition energies of the (HCN)···Li[24], and Na_nF_{n-1} ($n \leq 6$)[38] are lying in the range of 0.95−1.5 eV. For the hydrated electron cluster $(H_2O)_n^-$ ($n \rightarrow \infty$), the first transition energy is 1.977 or 1.947 eV.[19]

Notice that, this intercage electron localization transition leads to significant charge transfer Δq (for the calculation method, see Figure S2 in the Supporting Information) and large dipole moment change $\Delta\mu$. From Table 1, the large Δq values of e^-@AB and e^-@BB′ are 0.843 and 0.830, respectively. The large $\Delta\mu$ values are 24.540 D (e^-@AB) and 20.259 D (e^-@BB′).

The second, third, and fourth transitions correspond to s → p type excess electron orbital excitations. Exciting the excess electron from the ground state to the third excited state for the e^-@AB, the electron transition is from one cage to two cages (A → AB) with the transition energy of 2.193 eV. The other electron transitions are localized in one cage, i.e., cage A → A for e^-@AB and cage B → B for e^-@BB′. The ranges of the intracage transition energies of them are 1.870−2.220 eV and 2.119−2.417 eV for e^-@AB and e^-@BB′, respectively.

We can define the conditions for forming the intercage excess electron localization transition in a system as follows. (1) In the system, the number of the cages (or units) with the capability of confining excess electron is larger than that of the confined excess electron(s). (2) In the ground state the excess electron(s) are locally confined inside some cage(s) (or units) and the vacant cage(s) can locally confined the excess electron(s) in low-lying excited states. (3) According to the selection rule, the intercage excess electron localization transition is allowed. For the $e^-@C_{20}F_{20}$[28] and $e^-@C_{60}F_{60}$,[30] each of them is one-cage single molecule with one trapped excess electron. The number of the cages is equal to that of the confined excess electrons. As a result, there remains no vacant cage for the occurrence of the intercage transition. In the multicage many-electron crystalline electride of $(Ca_{24}Al_{28}O_{64})^{4+}(e^-)_4$, the concentration fraction of anionic electron is 1/3 per cage and the electron localization transitions of intercage s → s and intracage s → p occur.[27]

Notice that, considering the perfectly symmetry of the neutral molecule BB′, there should be a pair of the degenerate states for e^-@BB′ in the ground state as the excess electron is localized inside one of the identical cages (B or B′). The two degenerate states have the reversed directional intercage electron localization transitions (including the associated significant charge transfer manifested also by the large dipole moment changes).

Excess electron localization could be regulated by changing the molecular structure with cages. Selecting appropriate number of the cages (or units) and regulating the structures of the cages (or units) allow realize the electron transfer localization transition in a single multicage molecule.

Conclusion

In this paper, we have used double-cage structural molecule with large interior electronic attractive potential to confine an excess electron and obtained $e^-@C_{24}F_{22}(NH)_2C_{20}F_{18}$ and $e^-@C_{20}F_{18}(NH)_2C_{20}F_{18}$ for the first time. The electron localization is realized and the intercage electron transfer localization transition in a single molecule is discovered. This intercage electron transfer localization transition is companied with large charge transfer ($\Delta q > 0.8$) and large dipole moment change of the molecule ($\Delta\mu > 20$ D), which may relate to the high-performance molecular photophysical and photochemical properties as well as single molecular photoelectric devices.

We expect that this work may also promote the new multicage organic electride chemistry.

Acknowledgment. This work was supported by the National Natural Science Foundation of China (No. 20773046).

Supporting Information Available: Comparison of calculated results (in eV) between different method with 6-311+G* basis set for $(LiF)_6^{2-}$, the construction and the location of 4s4p and 6s6p4d diffuse basis sets, the three main vibration modes, the first transition energies of some systems with excess electrons, and calculation method of the intercage charge transfer. This material is available free of charge via the Internet at http://pubs.acs.org.

References and Notes

(1) Ahn, T. K.; Avenson, T. J.; Ballottari, M.; Cheng, Y.-C.; Niyogi, K. K.; Bassi, R.; Fleming, G. R. *Science* **2008**, *320*, 794–797.

(2) Tributsch, H.; Pohlmann, L. *Science* **1998**, *279*, 1891–1895.
(3) Seo, K.; Konchenko, A. V.; Lee, J.; Bang, G. S.; Lee, H. *J. Am. Chem. Soc.* **2008**, *130*, 2553–2559.
(4) Ma, D. L.; Che, C. M.; Yan, S. C. *J. Am. Chem. Soc.* **2009**, *131*, 1835–1846.
(5) Ito, S.; Miura, H.; Uchida, S.; Takata, M.; Sumioka, K.; Liska, P.; Comte, P.; Pechy, P.; Graetzel, M. *Chem. Commun.* **2008**, 5194–5196.
(6) Wang, P.; Zakeetuddin, S. M.; Moser, J. E.; Nazeeruddin, M. K.; Sekiguchi, T.; Grätzel, M. *Nat. Mater.* **2003**, *2*, 402–407.
(7) Senechal-David, K.; Hemeryck, A.; Tancrez, N.; Toupet, L.; Williams, J. A. G.; Ledoux, I.; Zyss, J.; Boucekkine, A.; Guegan, J. P.; Le Bozec, H.; Maury, O. *J. Am. Chem. Soc.* **2006**, *128*, 12243–12255.
(8) Akasaka, T.; Otsuki, J.; Araki, K. *Chem.—Eur. J.* **2002**, *8*, 130–136.
(9) De Cola, L.; Belser, P. *Coord. Chem. Rev.* **1998**, *177*, 301–346.
(10) Wand, Y.; Herron, N.; Grushin, V. V.; LeCloux, D. D.; Petrov, V. A. *Appl. Phys. Lett.* **2001**, *79*, 449–451.
(11) Tsuboyama, A.; Iwawaki, H.; Furugori, M.; Mukaide, T.; Kamatani, J.; Igawa, S.; Moriyama, T.; Miura, S.; Takiguchi, T.; Okada, S.; Hoshino, M.; Ueno, K. *J. Am. Chem. Soc.* **2003**, *125*, 12971–12979.
(12) Chen, Wei.; Li, Z.-R.; Li, Y.; Sun, C.-C.; Gu, F. L. *J. Am. Chem. Soc.* **2005**, *127*, 10977–10981.
(13) Muhannad, S.; Xu, H.; Liao, Y.; Kan, Y.; Su, Z. *J. Am. Chem. Soc.* **2009**, *131*, 11833–11840.
(14) Xu, H.-L.; Li, Z.-R.; Su, Z.-M.; Muhannad, S.; Gu, F. L.; Harigaya, K. *J. Phys. Chem. C* **2009**, *113*, 15380–15383.
(15) Paik, D. H.; Lee, I.-R.; Yang, D.-S.; Baskin, J. S.; Zewail, A. H. *Science* **2004**, *306*, 672–675.
(16) Hammer, N. I.; Shin, J.-W.; Headrick, J.; Diken, E. G.; Roscioli, J. R.; Weddle, G. H.; Johnson, M. A. *Science* **2004**, *306*, 675–679.
(17) Turi, L.; Sheu, W.-S.; Rossky, P. J. *Science* **2005**, *309*, 914–917.
(18) Verlet, J. R. R.; Bragg, A. E.; Kammrath, A.; Cheshnovsky, O.; Neumark, D. M. *Science* **2005**, *307*, 93–96.
(19) (a) Coe, J. V.; Williams, S. M.; Bowen, K. H. *Int. Rev. Phys. Chem.* **2008**, *27*, 27–51. (b) Simons, J. *J. Phys. Chem. A* **2008**, *112*, 6401–6511, and references therein.
(20) Desfrançois, C.; Carles, S.; Schermann, J. P. *Chem. Rev.* **2000**, *100*, 3943–3962.
(21) Page, C. C.; Moster, C. C.; Chen, X.; Dutton, L. *Nature (London)* **1999**, *402*, 47–52.
(22) Lee, H. M.; Lee, S.; Kim, K. S. *J. Chem. Phys.* **2003**, *119*, 187–194.
(23) Li, Y.; Li, Z.-R.; Wu, D.; Li, R.-Y.; Hao, X. Y.; Sun, C.-C. *J. Phys. Chem. B* **2004**, *108*, 3145–3148.
(24) Chen, W.; Li, Z.-R.; Wu, D.; Li, R.-Y.; Sun, C.-C. *J. Phys. Chem. B* **2005**, *109*, 601–608.
(25) (a) Matsuishi, S.; Toda, Y.; Miyakawa, M.; Hayashi, K.; Kamiya, T.; Hirano, M.; Tanaka, I.; Hosono, H. *Science* **2003**, *301*, 626–629. (b) Chiesa, M.; Paganini, M. C.; Giamello, E.; Murphy, D. M.; Di Valentin, C.; Pacchioni, G. *Acc. Chem. Res.* **2006**, *39*, 861–867. (c) Edwards, P. P.; Anderson, P. A.; Thomas, J. M. *Acc. Chem. Res.* **1996**, *29*, 23–29. (d) Srdanov, V. I.; Stucky, G. D.; Lippmaa, E.; Engelhardt, G. *Phys. Rev. Lett.* **1998**, *80*, 2449–2452.
(26) Miyakawa, M.; Kim, S. W.; Hirano, M.; Kohama, Y.; Kawaji, H.; Atake, T.; Ikegami, H.; Kono, K.; Hosono, H. *J. Am. Chem. Soc.* **2007**, *129*, 7270–7271.
(27) Sushko, P. V.; Shluger, A. L.; Hayashi, K.; Hirano, M.; Hosono, H. *Phys. Rev. Lett.* **2003**, *91*, 126401.
(28) Zhang, C.-Y.; Wu, H.-S.; Jiao, H. *J. Mol. Model.* **2007**, *13*, 499–503.
(29) Irikura, K. K. *J. Phys. Chem. A* **2008**, *112*, 983–988.
(30) Wang, Y.-F.; Li, Z.-R.; Wu, D.; Sun, C.-C.; Gu, F.-L. *J. Comput. Chem.* **2010**, *31*, 195–203.
(31) Wahl, F.; Weiler, A.; Landenberger, P.; Sackers, E.; Voss, T.; Haas, A.; Lieb, M.; Hunkler, D.; Wörth, J.; Knothe, L.; Prinzbach, H. *Chem.—Eur. J.* **2006**, *12*, 6255–6267.
(32) Shkrob, I. A. *J. Phys. Chem. A* **2007**, *111*, 5223–5231.
(33) Rienstra-Kiracofe, J. C.; Tschumper, G. S.; Schaefer, H. F., III; Sreela, N.; Ellison, G. B. *Chem. Rev.* **2002**, *102*, 231–282.
(34) Zhang, L.; Yan, S.; Cukier, R. I.; Bu, Y. *J. Phys. Chem. B* **2008**, *112*, 3767–3772.
(35) Likura, H.; Tsuneda, T.; Yanai, T.; Hirao, K. *J. Chem. Phys.* **2001**, *115*, 3540–3544.
(36) (a) Jordan, K. D.; Luken, W. *J. Chem. Phys.* **1976**, *64*, 2760–2766. (b) Skurski, P.; Gutowski, M.; Simons, J. *Int. J. Quantum Chem.* **2000**, *80*, 1024–1038. (c) Anusiewicz, I.; Skurski, P.; Simons, J. *J. Phys. Chem. A* **2002**, *106*, 10636–10644.
(37) Frisch, M. J., et al. *Gaussian 03, Revision E.01*; Gaussian, Inc.: Wallingford, CT, 2003; and*Gaussian 09, Revision A.02*; Gaussian, Inc.: Wallingford, CT, 2009.
(38) Durand, G.; Spiegelmann, F.; Poncharal, P. H.; Labastie, P.; L'Hermite, J.-M.; Sence, M. *J. Chem. Phys.* **1999**, *110*, 7884–7892.

JP1056557